Estimation of Aperture Errors with Direct Interferometer-Output Feedback for Spacecraft Formation Control

Hui-Ling Lu, Victor H. L. Cheng, Jesse A. Leitner, Richard G. Lyon, and Kenneth G. Carpenter

Abstract—Long-baseline space interferometers involving formation flying of multiple spacecraft hold great promise as future space missions for high-resolution imagery. The major challenge of obtaining high-quality interferometric synthesized images from long-baseline space interferometers is to control these spacecraft and their optics payloads in the specified configuration accurately. In this paper, we describe our effort toward fine control of long-baseline space interferometers without resorting to additional sensing equipment. We present an estimation procedure that effectively extracts relative x/y translational exit pupil aperture deviations from the raw interferometric image with small estimation errors.

I. INTRODUCTION

SPACE-BASED telescopes such as the Hubble Space Telescope have the advantage of avoiding atmospheric aberrations affecting ground-based telescopes. In general, a telescope with a larger aperture achieves finer angular resolution. The Hubble Space Telescope represents the largest financially feasible monolithic space telescope. Without resorting to one large expensive monolithic mirror, the James Webb Space Telescope [1], scheduled to be launched in 2011, has a larger aperture by using deployed segmented mirrors. To deliver even larger apertures for high-resolution imagery, long-baseline space interferometers are under extensive study. A long-baseline space interferometer consists of several spacecraft (including collectors, beam combiner or detector) formation-flying in a specified geometric configuration. A major challenge of obtaining high-quality interferometric synthesized images from long-baseline space interferometers is to control these spacecraft and their optics payloads in the specified configuration accurately.

In this paper, we describe our effort toward fine control of long-baseline space interferometers without resorting to additional sensing equipment. Here, the Stellar Imager (SI) [2] space interferometer mission concept is selected as the basis for algorithm evaluation.

Hui-Ling Lu and Victor H. L. Cheng are with Optimal Synthesis Inc., Palo Alto, California 94303, USA (e-mail: vicky@ optisyn.com).
Jesse A. Leitner, Richard G. Lyon and Kenneth G. Carpenter are with NASA Goddard Space Flight Center, Greenbelt, Maryland 20771, USA.

The SI is a Fizeau-type interferometer composed of 9 to 30 1-m-class spherical articulated mirrors on formation-flying satellites ("mirrorsats") and a central hub with focal-plane instrumentation, as depicted in Fig. 1. The objective of the SI mission is to obtain information on dynamo patterns for stars with Sun-like activity. The imager will operate at the UV/optical frequency range with angular resolution of 60 and 120 μ-arcsec at 1550 Å and 2800 Å, respectively. Its focal-plane resolution is expected to be on the order of 1000 total pixels (33×33) over the surface of nearby dwarf stars.
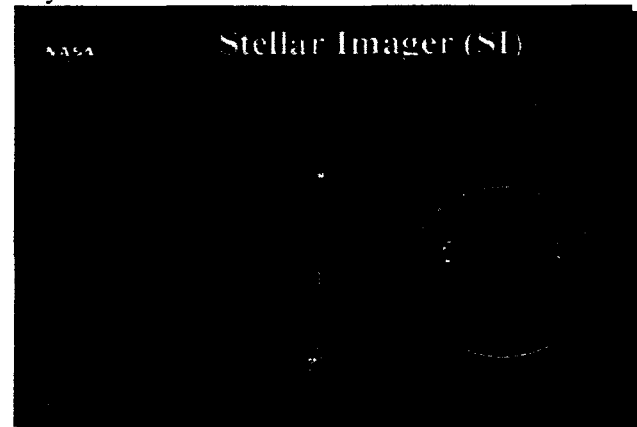

Fig. 1. The Stellar Imager Space Interferometer Mission Concept

In order to achieve high-quality images with the SI mission, the position and orientation of the articulated mirrors need to be aligned precisely on the larger (0.5-km diameter) virtual mirror surface to keep optical beams in phase. Each mirrorsat comes with 5 degrees of freedom of movement (tip, tilt, piston, as well as 2-D translations). The objective of our study is to control these mirrorsats using direct interferometer outputs. Fig. 2 shows the overall control concept. Deviations of these mirrorsats, χ, from the desired mirror surface are estimated from direct interferometer outputs including the raw image collected at the central hub and other measurements from metrology sensors. The Optical System Master Control driven by estimated deviations and measurements from the metrology instrumentation issues commands to the optical system components on the spacecraft, as well as feeds back data to the Spacecraft Formation Flying Control. The Spacecraft

Formation Flying Control in turn issues commands to control the collection of spacecraft. Data from the optical system on each spacecraft is also fed back to the Optical System Master Control to initiate coarse control when the fine control via estimated deviations $\hat{\chi}$ is not adequate. To control these mirrorsats in great precision, the first step is to obtain accurate estimates of mirrorsats deviations. In this paper, we would like to present our results of estimating the 2-D translation deviations of these mirrorsats using direct interferometric images.
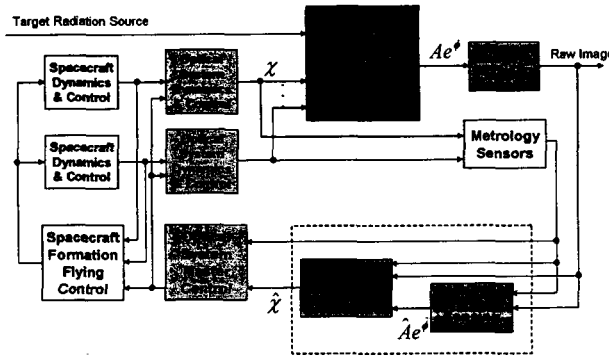

Fig. 2. Control Concept Block Diagram

II. PROBLEM FORMULATION

A. "Mirrorsat" Deviation and Interferometric Image

To infer deviations of these mirrorsats based on raw images, the relationship between the geometric configuration of these mirrors and the observed image is depicted in Fig. 3. It is assumed that these spherical mirrorsats are configured and controlled under a predefined control coordinate system. Each mirror has 5 degrees of freedom: x, y, z translation, and tip, tilt rotation. Geometric deviations of the mirrors are mapped into aperture deviations at the entrance pupil through a coordinate transformation. Under the assumption that there is perfect beam combination of the collected light beams from all mirrors, the aperture configuration at the exit pupil would be a scaled version of the one at the entrance pupil [3]. This implies that geometric deviations of these spherical mirrorsats can also be obtained from deviations of apertures at the exit pupil via a coordinate transformation. Deviations of the apertures include x, y, piston translational, and tip, tilt rotational errors. They are expressed by the wavefront error coordinate system [4], in which the piston variable points towards the focal point of the optical system.

In the image domain, the properties of the optical system can be described by a point spread function (PSF). The PSF is related to the phase at these exit pupil apertures through a Fourier transform [4]. More precisely, a PSF can be derived

as the magnitude-squared of the Fourier transform of a complex pupil function Ae^{ϕ}. Deviations of exit pupil apertures are then shown as distortions from the ideal PSF. In addition to the PSF, the modulation transfer function (MTF) defined as the magnitude of the Fourier Transform of the PSF is used to evaluate properties of the optical system. Since the definition of the control coordinate of SI is not yet complete, we have focused on estimating the exit pupil aperture deviations from the interferometric raw image resulting from the PSF convolved with the target source. In addition, since the estimation is based on the raw image, deviations of "mirrorsats" are assumed to be small enough to provide reasonably focused images.
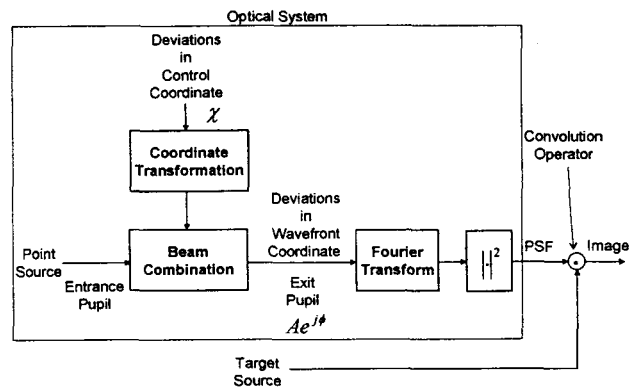

Fig. 3. Optical System Modeling Showing Relationship Between "Mirrorsat" Deviation and Interferometric Output Image

B. MTF and Baselines

To position mirrorsats correctly, the baseline of each mirrorsat pair, defined as the separation of the pair's center locations at the exit pupil plane, needs to be maintained. It turns out that one can extract the baseline information from the MTF.

$$PSF_{two}(\theta) = 2PSF_{one}(\theta) \cdot [1 + \cos(2\pi \cdot \theta \cdot B / \lambda)]$$
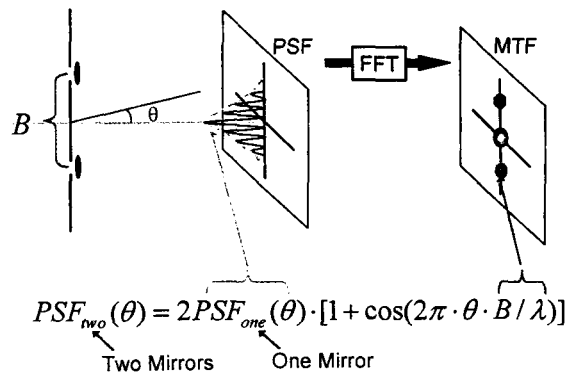
Two Mirrors   One Mirror

Fig. 4. PSF and MTF of a 2-Element Interferometer

A simple 2-element interferometer illustrates the relationship between the MTF and the baseline. Fig. 4

illustrates the PSF and MTF of a 2-element interferometer [5]. The 2-mirror PSF is a 1-mirror PSF modulated with fringes. The 1-mirror PSF is essentially the diffraction pattern of a single mirror. Assume that the size of the mirror is much smaller than the baseline of the interferometer, so that there are multiple fringe cycles within the 1-mirror PSF envelope. In the frequency domain, the MTF will consist of three distinct modes, which are observed as three dots in a pseudo-color depiction of the function. The base-band dot corresponds to the 1-mirror MTF and the other two are just translated versions of the 1-mirror MTF due to fringe modulation.
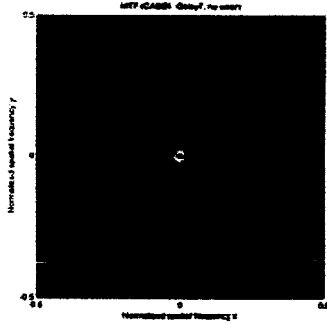

Fig. 5. MTF of Golay-7 Configuration

A Golay configuration, which is considered by the SI mission, is an aperture configuration for sparse interferometric arrays optimized to minimize redundant baselines. Fig. 5 shows the MTF of a Golay-7 configuration [6]. The simulated configuration consists of 7 circular apertures with diameter equal to 0.0125 meter. The shortest baseline is 0.0254 m, which is about twice the diameter of each aperture. These baselines are large enough that the MTF dots are visibly separable. Since the spatial frequency of the fringes is related to the size and the direction of the baseline, the positions of these MTF dots contain information on the size and orientation of the baselines. Moreover, it is observed that the piston errors and the tip, tilt errors alter the shapes of the MTF dots, but they do not seem to affect the locations of their "centroids." Hence, under the assumption that baselines are much larger than the diameter of individual mirrors, baseline deviations can be estimated from the centroid deviations of the MTF dots. For a non-redundant constellation such as the Golay configuration, the estimated baseline information can be used to estimate aperture deviations.

C. Baselines and Translational Deviations

In fact, the baseline error is a linear transformation of the x/y translational deviation. Let us define the baseline pattern $\overline{b}_i$ for the mirror #i as the collection of the MTF dots corresponding to all the baselines connected to the mirror #i. For example, Fig. 6 shows baseline patterns of the Golay-7 configuration as red dots for individual

mirrors. If one numbers all positive MTF dots in sequence, the baseline pattern $\overline{b}_i$ can be denoted as a column vector, such as $\begin{bmatrix} 1 & 0 & 1 & \cdots & 0 & 1 \end{bmatrix}^T$, where 1's indicate all MTF dots corresponding to baselines connected to the mirror #i. Assuming that there are N mirrors and therefore $M = N \cdot (N-1)/2$ baselines, the relationship between the baseline error and the x/y translational deviation can be written as

$$\begin{bmatrix} \overline{b}_1 & \cdots & \overline{b}_N \end{bmatrix} \begin{bmatrix} \Delta x_1 \\ \vdots \\ \Delta x_N \end{bmatrix} = \begin{bmatrix} \Delta x_1' \\ \vdots \\ \Delta x_M' \end{bmatrix} \text{ or } A \cdot X = Y. \quad (1)$$

X represents the translational error in the exit pupil plane either along the x axis or the y axis. Similarly, Y represents the baseline error either along the x axis or the y axis. Since the MTF only retains the baseline information, matrix A has rank $N-1$. That is, only $N-1$ independent variables can be recovered. One can reduce the number of independent variables by selecting a mirror as the reference mirror and estimate the relative deviations of other apertures with respect to the reference mirror. That is,

$$Y = A \cdot X = \begin{bmatrix} U_1 & U_2 \end{bmatrix} \begin{bmatrix} \Sigma_1 & 0 \\ 0 & 0 \end{bmatrix} \begin{bmatrix} V_1^T \\ V_2^T \end{bmatrix} X = U_1 \Sigma_1 V_1^T X$$

$$= U_1 \Sigma_1 \begin{bmatrix} V_{11}^T & \vdots & V_{12}^T \end{bmatrix} \begin{bmatrix} 0 \\ \cdots \\ X_2 \\ \vdots \\ X_N \end{bmatrix} = U_1 \Sigma_1 V_{12}^T \begin{bmatrix} X_2 \\ \vdots \\ X_N \end{bmatrix} = A' \begin{bmatrix} X_2 \\ \vdots \\ X_N \end{bmatrix} \quad (2)$$

where A' is a well-conditioned matrix of rank $N-1$, and the relative aperture deviations can be obtained by the following equation.

$$\begin{bmatrix} X_2 & \cdots & X_N \end{bmatrix}^T = (A'^T A')^{-1} \cdot A'^T Y \quad (3)$$
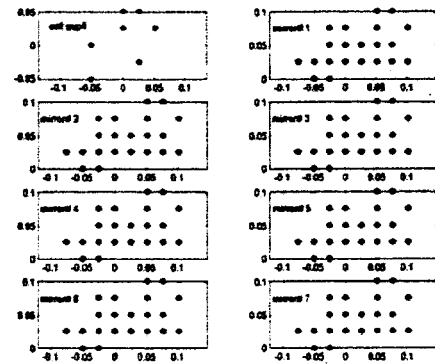

Fig. 6. Baseline Patterns of Individual Mirrors

In summary, the centroid of an MTF dot is a prominent feature that has the potential to be used for determining the relative deviation of the center of the aperture on the exit pupil plane. However, with the only available raw image

whose Fourier Transform is a noisy version of the true MTF, a robust centroid estimation algorithm is needed. The following section describes the overall estimation procedure that we developed for extracting relative x/y translational aperture deviations from the raw interferometric image.

III. ESTIMATION PROCEDURE

An effective estimation procedure using a k-means clustering [7] technique and least-squares ellipse fitting [8], [9] is developed. The objective of the estimation is to calculate x/y translational deviations of exit pupil apertures so that every baseline is precisely maintained. Once every baseline is controlled at the predefined location, the PSF is known and the target image can be inverse-filtered from the measured raw image if there are no other deviations.
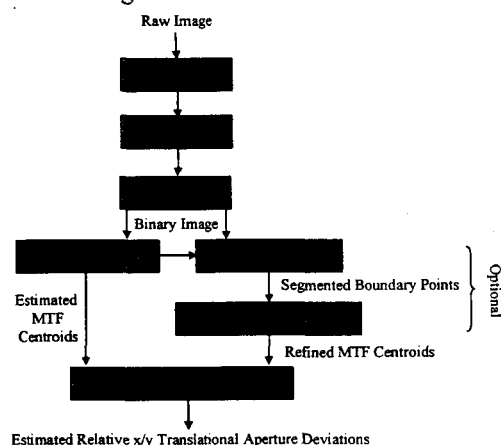
Fig. 7. Estimation Procedure

Fig. 7 depicts the flowchart of the estimation procedure. First, the Fourier Transform of the raw image is taken to approximate the MTF of the interferometric system. The DC portion of the approximated MTF is removed to amplify the MTF dots containing the baseline information. Second, thresholding is performed to convert the resulting image into a binary image. The thresholding value is selected by the criterion that 90% of the total energy is preserved. The next step of the estimation is to calculate the x/y translational deviations of the baselines from the thresholded binary image. Locations of the baselines are estimated as center locations of the MTF dots. Three different methods have been tried to estimate the MTF centers: k-means clustering, direct least-squares ellipse fitting and weighted least-squares ellipse fitting. Initialized with the desired baseline locations, k-means clustering estimates the centers of the MTF dots from binary image data points. One can further refine the center estimation of each MTF dot by the direct least-squares ellipse fitting or the weighted least-squares ellipse fitting method. Segmented boundary points belonging to different MTF

dots are obtained via the boundary extraction and k-means clustering. Using these segmented data points, ellipse fitting methods calculate the center of each MTF dot. The weighted least-squares ellipse fitting is a variation of the least-squares ellipse fitting, where each data point is weighted according to its MTF magnitude. Finally, with one aperture selected as the reference, deviations of other apertures can be obtained from deviations of baselines through a linear transformation as shown in (3).

IV. RESULTS AND DISCUSSIONS

To illustrate the effectiveness of the proposed estimation procedure, we would like to walk through an example of extracting the relative x/y translational exit pupil aperture deviations from a realistic simulated interferometric raw image.
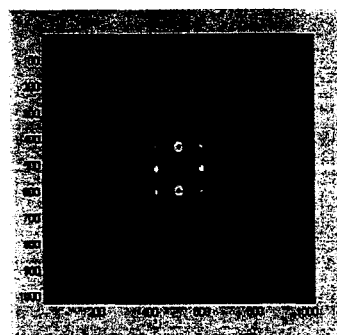
Fig. 8. Simulated DC-Blocked Interferometric Image of Sun Source in Frequency Domain
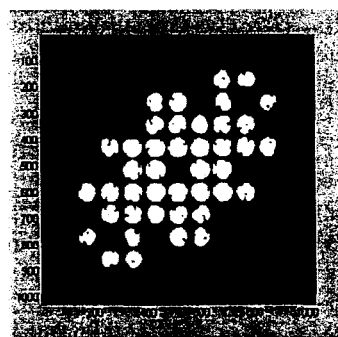
Fig. 9. Binary Image of Fourier Transform of the Raw Image

The raw image was simulated by convolving a model image of the Sun in the light of CIV atoms (1550 Å transitions) with the point spread function generated using the Golay-7 configuration. The Sun image is reduced to the size of 30×30 pixels using Wavelet transform [10]. Fig. 8 shows the simulated raw image in the frequency domain with the base band removed. Fig. 9 shows the binary image after thresholding. Fig. 10 shows the extracted boundaries of this binary image. Fig. 11 shows the segmented boundary points after the application of k-means clustering. Every boundary point depicted by a different color is segmented to belong to a certain MTF dot. The estimated

center (x) and desired center locations (o) are also shown. Fig. 12 shows the baseline estimation result and Fig. 13 shows the estimation results of aperture locations with aperture #1 as the reference.
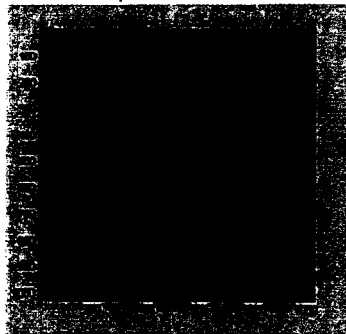

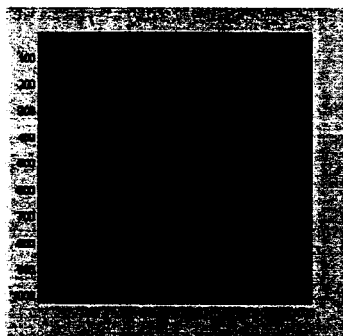Fig. 10. Boundaries of the Thresholded Binary Image

Fig. 11. Segmented Boundary Points After k-Means Clustering
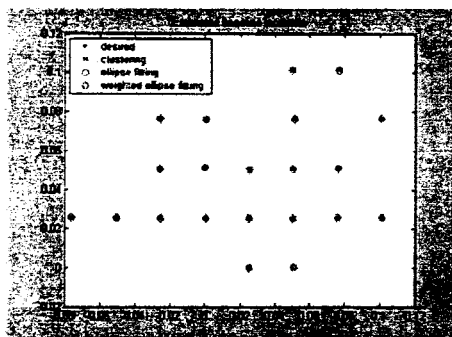

Fig. 12. Estimated Baseline Locations

To test the robustness of the proposed estimation procedure, Fig. 14 depicts baseline estimation errors of 100 runs. Errors have been normalized in terms of pixels, where each pixel is equivalent to 0.0002976 m. The Sun image with the size of 30×30 pixels is used as the extended source. Center locations of the exit pupil apertures are randomly deviated from the desired Golay-7 configuration with standard deviation of 0.001 m. The upper plot in Fig. 14 shows the average magnitude of the baseline estimation error for each run. The bottom plot shows the maximum magnitude of the baseline estimation error for each run. The average magnitudes of the simulated deviations are

also overlapped on the plots. In this case, weighted least-squares ellipse fitting appears to be the most robust method to estimate baseline centers. Table 1 summarizes the average baseline estimation error of 100 runs for both the extended source and the point source. It shows that the extended source affects the estimation accuracy substantially.
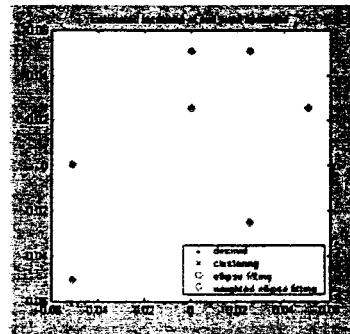

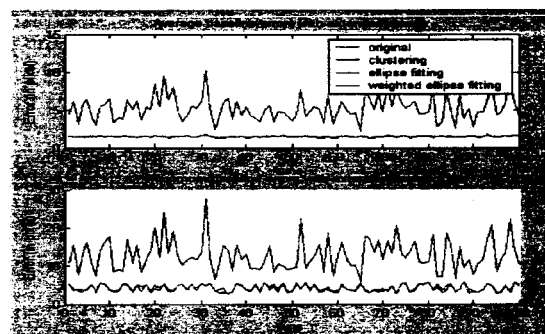Fig. 13. Estimated Locations of Exit Pupil Apertures

Fig. 14. Average Baseline Estimation Errors

Table 1. Average Baseline Estimation Error with Location Deviations

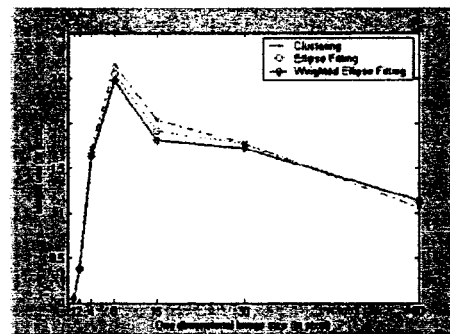| Method\Source Type	Extended Source	Point Source
k-Means Clustering	1.436	0.0223
Least-Squares Ellipse Fitting	1.390	0.0342
Weighted Ellipse Fitting	1.363	0.0551

Fig. 15. Average Baseline Estimation Errors w.r.t. Image Size

We have also evaluated the performance of the proposed estimation procedure with respect to different image

sources and image sizes. Fig. 15 shows the average baseline estimation errors with respect to different image sizes. The x-axis represents the one-dimensional image size in pixels. All test images are square images. The average baseline estimation errors are averaged across simulated images of the Sun representing 100 sequential rotational phases. The original simulated Sun images have the size of 120×120 pixels. Wavelet decomposition and reconstruction are performed to obtain test images with reduced sizes. The performance of the estimation would improve if the frequency response of the extended source is closer to that of the point source. However, a smaller extended source does not readily imply a flatter frequency response.

To confirm our observation that piston errors and x-tilt errors alter the shapes of the MTF dots without affecting their "centroids," we investigated the impact of piston and x-tilt deviations upon the baseline estimation errors. Several snapshots of the Sun image sequence are randomly selected to run the following experiments. There is no x/y translation deviation in this case. The Golay-7 configuration is used to layout the desired locations of the exit-pupil apertures. The standard deviation of the piston error ranges from 0.2π to π. The standard deviation of the x-tilt deviation ranges from $10\lambda/D$ to $30\ \lambda/D$. In our experiments, the average baseline estimation errors for each image source do not change with respect to the piston and x-tilt deviations at all.
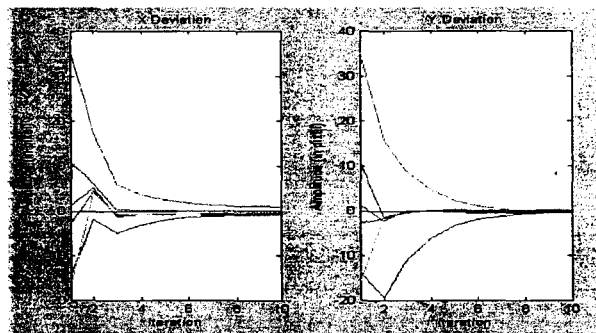

Fig. 16. One Control Example Using k-means Clustering

Fig. 16 shows one control example of using k-means clustering method to estimate the translation deviations. Here, we assume that we have perfect actuators which can move the mirrors precisely. The left-hand-side plot depicts the average x translation deviations. The right-hand-side plot depicts the average y deviations. Within 10 iterations, translation deviations have shown good convergence. The maximum baseline error is 1.4 pixels at convergence. The maximum x deviation is 1.01 pixels and the maximum y deviation is -0.47 pixels.

V. CONCLUSION

Long-baseline space interferometers involving formation

flying of multiple spacecraft hold great promise as future space missions for obtaining high-resolution imagery. The major challenge of obtaining high-quality interferometric synthesized images from long-baseline space interferometers is to control these spacecraft and their optics payloads in the specified configuration accurately. In this paper, we describe our effort toward fine control of long-baseline space interferometers without resorting to additional sensing equipment. We present an estimation procedure that effectively extracts relative x/y translational exit pupil aperture deviations from the raw interferometric image. The proposed estimation procedure was tested under different types of mirror deviations and it shows that the baseline estimation errors are no larger than 2 pixels of the raw image in most scenarios. In order to provide control with 5 degrees of freedom, we are evaluating phase diversity methods [11], [12] to estimate tip, tilt and piston deviations. Iteratively running the x/y translation estimation and the phase diversity method is very likely to improve the estimation of aperture deviations. Our x/y translational estimation results can be used to estimate the mask functions, which are used in the phase diversity estimation. Since the phase diversity method provides an estimate of the source image, a better MTF estimate can be obtained and in turn be used to estimate x/y translational deviations.

REFERENCES

[1] James Webb Space Telescope, website http://www.jwst.nasa.gov/.
[2] K. G. Carpenter, et al., "The stellar imager (SI) mission concept," *Proc. SPIE* 4854, 2002.
[3] J. E. Harvey, P. R. Silverglate, and A. B. Wissinger, "Optical performance of synthetic aperture telescope configurations," *Southwest Conference in Optics*, pp. 110–118, SPIE Vol. 540, 1985.
[4] W. Goodman, *Introduction to Fourier Optics*, McGraw-Hill Inc., 1996.
[5] S.-J. Chung, "Design, implementation and control of a sparse aperture imaging satellite," *Master of Science Thesis*, Department of Aeronautics and Astronautics, MIT, 2002.
[6] M. Golay, "Point arrays having compact non-redundant autocorrelations," *J. Opt Soc. Am.*, Vol. 61, pp. 272, 1971.
[7] David Corney, "the Clustering toolbox," Computer Science Dept., University College London, 2000. Available: http://www.cs.ucl.ac.uk/staff/D.Corney/ClusteringMatlab.html
[8] A. Fitzgibbon, M. Pilu , and R. B. Fisher, "Direct least-square fitting of Ellipses," *IEEE Trans. on Pattern Anaylsis and Machine intelligence*, Vol. 21, No. 5, May 1999. Available: http://www.hpl.hp.co.uk/people/mp/research/ellipse.htm.
[9] R. Halíř and J. Flusser, "Numerically stable direct least squares fitting of ellipses," *In the 6th Int. Conf. in Central Europe on Computer Graphics and Visualization.*, Plzen, Czech Republic, 1998.
[10] S. Mallat, *A wavelet tour of signal processing*. Academic Press, San Diego, 1999.
[11] R. G. Lyon, J. E. Dorband, T. Murphy, and G. Solyar, "Overview: computational complexity and space based optical systems," *Proceedings of the Workshop on Computational Optic and Imaging for Space Applications*, pp. 1–9, NASA Goddard Space Flight Center, May 10–12, 2000.
[12] M. G. Löfdahl and G. B. Scharmer, "Wavefront sensing and image restoration from focused ad defocused solar images," *Astronomy & Astrophysics Supplement Series* 107, pp. 243-264, 1994.